Reception of LoRa Signals From LEO Satellites

Reception of LoRa Signals From LEO Satellites

GIULIO COLAVOLPE, Senior Member, IEEE

TOMMASO FOGGI
MICHELANGELO RICCIULLI
YURI ZANETTINI
University of Parma, Parma, Italy

JUAN-PEDRO MEDIANO-ALAMEDA
Inmarsat, London, U.K.

In this paper, the detection of LoRa signals from a low-earth orbit (LEO) satellite is considered. The use of a LEO satellite to collect messages from the terminals, as an alternative to terrestrial base stations in rural areas, represents a major challenge due to the specific impairments of this scenario, e.g., Doppler effects and interfering signals. A redesign, whose validation is assessed through a system simulator operating in a realistic scenario, is thus required.

Manuscript received March 17, 2018; revised October 18, 2018 and March 19, 2019; released for publication March 22, 2019. Date of publication April 9, 2019; date of current version December 5, 2019.

DOI. No. 10.1109/TAES.2019.2909336

Refereeing of this contribution was handled by V. Weerackody.

This work was supported by Inmarsat.

Authors' addresses: G. Colavolpe is with the Dipartimento di Ingegneria e Architettura and the CNIT Research Unit, University of Parma, I-43124 Parma, Italy, E-mail: (giulio.colavolpe@unipr.it); T. Foggi is with the CNIT Research Unit, University of Parma, I-43124 Parma, Italy, E-mail: (tommaso.foggi@nemo.unipr.it); M. Ricciulli and Y. Zanettini are with the Dipartimento di Ingegneria e Architettura, University of Parma, I-43124 Parma, Italy, E-mail: (michelangelo.ricciulli@nokia.com; y.zanettini@gmail.com); J.-P. Mediano-Alameda is with Inmarsat, EC1Y 1B London, U.K., E-mail: (jp.mediano@inmarsat.com). *(Corresponding author: Tommaso Foggi.)*

I. INTRODUCTION

In recent years, Internet of things (IoT) is developing at an impressive speed. Several lightweight protocols are already available for IoT devices, operating in the industrial, scientific and medical (ISM) band, among which the most popular are Sigfox and LoRaWAN (long range wireless area network) [1]. However, the need to install terrestrial base transceiver stations (BTS) represents a relevant drawback in the network deployment progress and, furthermore, it is likely that terrestrial coverage for these networks will never extend much beyond urban areas.

A possible solution to the specific problem of deployment speed and coverage area of these networks can be the provision of a low-earth orbit (LEO) constellation of satellites. We consider LEO satellites for the following main reasons: 1) global coverage, as geostationary satellites do not cover poles; 2) link budget, as the attenuation due to propagation distance is much smaller for LEO satellites; and 3) cost, as very cheap CubeSats can be employed for this purpose. Such LEO constellation will act as a gateway, by ensuring an alternative way to collect data coming from the end-devices to the central network server where no terrestrial coverage exists. The collected data can be stored on board and transmitted later to the central server when the latter falls in the satellite field of view.

Given the remarkable difference between the common terrestrial channel and the novel expected link, the design of a receiver suitable to be employed on a LEO satellite operating in the ISM band is of fundamental importance, since it must be able to detect messages coming from existing conventional IoT terrestrial terminals, which clearly will continue to see an unmodified network, while their signals will be processed by a LEO satellite. The design of this LEO satellite receiver will be addressed in this paper by taking into account the peculiar impairments of the satellite link that affect the performance of conventional receivers. In particular, the presence of significant Doppler effects related to the satellite movements have to be taken into account since they will significantly degrade the performance of a receiver designed for terrestrial use. In addition, the coverage area of a LEO satellite will be much wider than a possible terrestrial cell. This means that a larger amount of collisions of messages coming from terrestrial terminals have to be coped with. Techniques for interference mitigation thus have to be considered. Hence, in this IoT scenario, where we employ a satellite to collect packets from the IoT terminals, avoiding the deployment of terrestrial BTS, we need to design an advanced satellite receiver able to cope with the presence of significant Doppler shift and Doppler rate and the increased interference. The design of this receiver is the main contribution of this paper. Clearly, on the downlink side, an unmodified CT will hardly be able to detect a packet transmitted from a LEO satellite but this is not a significant limitation in this scenario, where the valuable information is that collected from the IoT terminals. We will thus assume that the IoT terminals are left unchanged,

with at most an upgrade of the deployed antenna, in order to improve the link budget.

In this paper, we concentrate on LoRa protocol which, unlike Sigfox, is publicly available. We will thus assume that the IoT terminal, client terminal (CT) in the following, falls outside the coverage area of terrestrial BTSs. The communication can thus be managed by a LEO satellite which acts as a gateway towards the radio access network (RAN). At this point, two different options can be considered—the signal detection can be either performed on board of the satellite, or the received signal can be just forwarded to be detected on ground. Nevertheless, the design of the receiver is independent of the preferred option if the link from the satellite to ground is assumed to be error-free—the choice on the position of the proposed receiver, on board or on ground, depends on the overall complexity constraints on board the satellite. We will first design and optimize a receiver able to cope with the mentioned impairments related to the LEO scenario. In order to validate the receiver design, we will also develop a system simulator able to assess the receiver performance in a realistic scenario.

The paper is organized as follows. Section II describes the LoRa signal model. The properties of this signal, to be exploited in the receiver design, are also described. The receiver design is addressed in Section III whereas Section IV gives details on the development of the system simulator which was used to assess the receiver performance. Section V reports the numerical results and, finally, conclusions are drawn in Section VI.

II. COMPLEX ENVELOPE OF A LORA SIGNAL

The complex envelope of a LoRa signal can be expressed as

$$s(t)=\sqrt{\frac{2E_{\mathrm{s}}}{T}}\exp\left\{j2\pi B\int_{-\infty}^{t}\left[\sum_{k}\Gamma(\tau-kT;a_k)\right]d\tau\right\} \tag{1}$$

where E_{s} is the energy per information symbol, T the symbol interval, B a proper parameter ($B=125$, 250, or 500 kHz in the LoRaWAN standard), $\{a_k\}$ the transmitted symbols belonging to the alphabet $\{0,1,\ldots,N-1\}$, N being a power of two, and $\Gamma(\tau;a_k)$ a function with support in $[-\frac{T}{2},\frac{T}{2}]$ having the expression

$$\Gamma(\tau;a_k)=\mathrm{mod}\left(\frac{\tau-a_kT/N}{T}+\frac{1}{2}\right)-\frac{1}{2}\quad -\frac{T}{2}\le\tau\le\frac{T}{2}. \tag{2}$$

In (2), the mod$(\cdot)$ function is the modulo operation in [0,1). We will define $\mathrm{SF}=\log_2 N$ the so-called *spreading factor* ($7\le\mathrm{SF}\le 12$ in the LoRaWAN standard). Parameters B, N, and T are related through the equation $BT=N=2^{\mathrm{SF}}$.

This modulation format shows some important properties—it has a constant envelope (and thus, it is insensitive to nonlinear distortions), a continuous phase (and thus, its spectrum is compact), no memory, and the occupied bandwidth is B (with good approximation). The constant envelope and the continuous phase can be simply verified from the complex envelope expression (1). From the definition of $\Gamma(t;a_k)$ in (2) we can also easily verify that the integral of $\Gamma(t;a_k)$ is zero, no matter the value of a_k. Thus, if we consider the interval $[kT-T/2,kT+T/2]$, the phase of the complex envelope will be the same at the beginning and at the end of the interval. This modulation is thus memoryless. Hence, the complex envelope can be expressed as

$$s(t)=\sum_{k}\xi(t-kT;a_k) \tag{3}$$

where $\xi(t-kT;a_k)$ is the slice of signal, with support in $[kT-T/2,kT+T/2]$, corresponding to symbol a_k and has the expression

$$\xi(t-kT;a_k)=\sqrt{\frac{2E_{\mathrm{s}}}{T}}\exp\left\{j2\pi B\int_{kT-T/2}^{t}\Gamma(\tau-kT;a_k)\,d\tau\right\}.$$

The closed-form expression of the power spectral density of (3) is composed of a continuous part $W_c(f)$ and a discrete part $W_\delta(f)$ made of a modulated Dirac delta train (see [2])

$$W_s(f)=W_c(f)+W_\delta(f)$$

where

$$W_c(f)=\frac{1}{T}\left[\frac{1}{N}\sum_{a_k}|\Xi(f;a_k)|^2-\left|\frac{1}{N}\sum_{a_k}\Xi(f;a_k)\right|^2\right]$$

and

$$W_\delta(f)=\frac{1}{N^2T^2}\sum_{n=-\infty}^{\infty}\left|\sum_{i}\Xi\left(\frac{n}{T};a_i\right)\right|^2\delta\left(f-\frac{n}{T}\right)$$

having denoted by $\Xi(f;a_k)$ the Fourier transform of $\xi(t;a_k)$ whose closed-form expression is

$$\begin{aligned}\Xi(f;a_k)=&\sqrt{\frac{E_{\mathrm{s}}T}{N}}e^{j2\pi B\left(\frac{3T}{8}-\frac{T}{2}\left(\frac{a_k}{N}+\left(+\frac{a_k}{N}-1+\frac{f}{B}\right)^2\right)\right)}\\&\cdot\left\{Z\left[\sqrt{2N}\left(+\frac{1}{2}-\frac{f}{B}\right)\right]-Z\left[\sqrt{2N}\left(-\frac{a_k}{N}+\frac{1}{2}-\frac{f}{B}\right)\right]\right\}\\&+\sqrt{\frac{E_{\mathrm{s}}T}{N}}e^{j2\pi B\left(-\frac{T}{8}+\frac{T}{2}\left(\frac{a_k}{N}+\left(\frac{a_k}{N}+\frac{f}{B}\right)^2\right)\right)}\\&\cdot\left\{Z\left[\sqrt{2N}\left(-\frac{a_k}{N}+\frac{1}{2}-\frac{f}{B}\right)\right]-Z\left[\sqrt{2N}\left(-\frac{1}{2}-\frac{f}{B}\right)\right]\right\}\end{aligned} \tag{4}$$

where $Z(\cdot)=C(\cdot)+jS(\cdot)$, $C(x)=\int_0^x\cos(\frac{\pi}{2}y^2)dy$ and $S(x)=\int_0^x\sin(\frac{\pi}{2}y^2)dy$ are the Fresnel integrals [3]. Fig. 1 reports the continuous part $W_c(f)$ of the power spectral density of LoRa signals for SF = 7 and 12. From this figure, we can see that a significant portion of the power is in the frequency range $[-\frac{B}{2},\frac{B}{2}]$ (thus the bandwidth of the corresponding passband signal is B).

It can be easily shown that we may express

$$\Gamma(t;a_k)=\Gamma(t;0)+\Phi(t;a_k)$$

i.e., as a first contribution which is the value of $\Gamma(t;a_k)$ corresponding to symbol $a_k=0$, thus common to all terms,

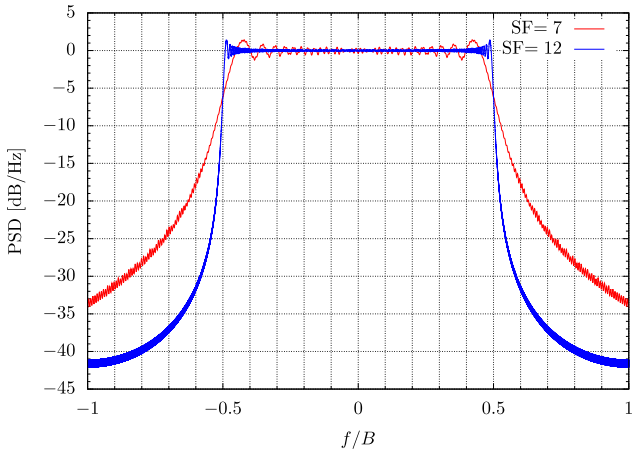

Fig. 1. Continuous part $W_c(f)$ of the power spectral density of LoRa signals for SF = 7 and SF = 12.

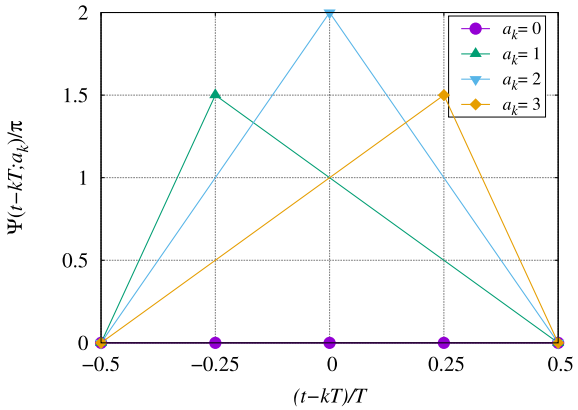

Fig. 2. Function $\Psi(t;a_k)$ for different values of a_k in the case SF = 2.

plus a second term which depends on a_k and can be expressed as

$$\Phi(t;a_k)=\begin{cases}-\frac{a_k}{N}+1 & \text{for } -\frac{T}{2}\le t\le -\frac{T}{2}+\frac{a_kT}{N}\\ -\frac{a_k}{N} & \text{for } -\frac{T}{2}+\frac{a_kT}{N}< t\le \frac{T}{2}\end{cases}. \quad (5)$$

$\Phi(t;a_k)$ is thus a piecewise constant. Hence, the complex envelope of a LoRa signal in the generic interval $[kT - T/2, kT + T/2]$ (and thus, the slice of signal we called $\xi(t-kT;a_k)$) can be equivalently expressed as

$$\xi(t-kT;a_k) = \xi(t-kT;0)\exp\left\{j2\pi B\int_{kT-T/2}^{t}\Phi(\tau-kT;a_k)\,d\tau\right\} \quad (6)$$

where

$$\xi(t-kT;0)=\sqrt{\frac{2E_s}{T}}\exp \times\left\{j2\pi B\int_{kT-T/2}^{t}\Gamma(\tau-kT;0)\,d\tau\right\} \quad (7)$$

is the slice of signal corresponding to $a_k = 0$ and is a term whose phase quadratically depends on t. It is called an *up-chirp signal*. We can define

$$\Psi(t-kT;a_k)=2\pi B\int_{kT-T/2}^{t}\Phi(\tau-kT;a_k)\,d\tau$$

obtaining

$$\xi(t-kT;a_k)=\xi(t-kT;0)\exp\{j\Psi(t-kT;a_k)\}.$$

The shape of $\Psi(t;a_k)$ is shown in Fig. 2 for SF = 2. Let us consider again the generic interval $[kT - T/2, kT + T/2]$. The slices $\xi(t-kT;a_k)$ corresponding to different symbols a_k are not orthogonal. This can be simply verified by computing the $N \times N$ matrix $\mathbf{A}$ whose elements are defined as

$$A_{i,\ell}=\frac{T}{2E_s}\int_{kT-T/2}^{kT+T/2}\xi(t-kT;a_k=i) \times\xi^*(t-kT;a_k=\ell)\,dt.$$

If the slices $\xi(t-kT;a_k)$ were orthogonal, $\mathbf{A}$ would be the identity matrix. So, in order to understand how far this matrix is from the identity one, we computed the normalized distance $\frac{1}{N}\|\mathbf{A}-\mathbf{I}\|_F$ where $\mathbf{I}$ is the $N \times N$ identity matrix and $\|\cdot\|_F$ is the Frobenius norm. It can be found that $1.1\cdot10^{-3}\le\frac{1}{N}\|\mathbf{A}-\mathbf{I}\|_F\le 2.1\cdot10^{-1}$ for $2\le \text{SF}\le 12$. We may thus conclude that the slices $\xi(t-kT;a_k)$ are not strictly orthogonal but can be approximated as such.

We said that signal $s(t)$ has (approximately) a bandwidth $B/2$. It can be thus reconstructed from its samples when using a sampling frequency $F_s = B = N/T$. Without loss of generality, we can consider the interval $[-T/2, T/2]$, i.e., $k = 0$, and thus, the transmission of symbol $a_k = a_0$. For $n=-\frac{N}{2},-\frac{N}{2}+1,\dots 0,\dots,\frac{N}{2}-1$, the N samples of the complex envelope are

$$\xi\left(\frac{nT}{N};a_0\right)=\xi\left(\frac{nT}{N};a_0=0\right)\exp\left\{j\Psi\left(\frac{nT}{N};a_0\right)\right\}.$$

By unwrapping the phase $\Psi\left(\frac{nT}{N};a_0\right)$, it can be easily verified that[1]

$$\exp\left\{j\Psi\left(\frac{nT}{N};a_0\right)\right\}=\exp\left\{-j\frac{2\pi}{N}a_0\left(n+\frac{N}{2}\right)\right\}$$

and thus

$$\xi\left(\frac{nT}{N};a_0\right)=\xi\left(\frac{nT}{N};a_0=0\right)\exp\left\{-j\frac{2\pi}{N}a_0\left(n+\frac{N}{2}\right)\right\}$$

or, equivalently

$$\xi_n(a_0)=\xi_n(a_0=0)\exp\left\{-j\frac{2\pi}{N}a_0n\right\}, \times n=0,1,\dots,N-1 \quad (8)$$

[1]Please notice that the equality holds for the samples only and not for the continuous-time signal.

having defined

$$\xi_n(a_0) = \xi\left(\frac{nT}{N}; a_0\right).$$

In other words, we can write the samples as the product of a discrete-time up-chirp signal, common to all signals, and a term whose phase is linearly decreasing with a slope depending on the transmitted symbol. These discrete-time samples are, this time, orthogonal. In fact

$$\sum_{n=0}^{N-1} \xi_n(a_0 = i)\xi_n^*(a_0 = \ell) = \begin{cases} N & i = \ell \\ 0 & i \neq \ell \end{cases}.$$

This property will be used later. It is important to notice that if we sample with a lower or higher sample frequency, this property no more holds, i.e., we can still write the samples as the product of an up-chirp signal, common to all signals, and a second term depending on the transmitted symbol, but this time the phase of this second term is no more linearly decreasing.

III. RECEIVER DESIGN

A. Detection Over an Additive White Gaussian Noise (AWGN) Channel

Let us assume that an uncoded LoRa signal is transmitted over an AWGN channel and that ideal synchronization has been performed (synchronization issues will be discussed in Section III-C). Without loss of generality, since the modulation is memoryless, as discussed in the previous section, we can consider the interval $[-T/2, T/2]$ focusing on the detection of symbol a_0 only. The complex envelope of the received signal can thus be expressed as

$$r(t) = \xi(t; a_0) + w(t)$$

where $w(t)$ is the complex envelope of an AWGN process with independent real and imaginary components having zero mean and power spectral density N_0.

From a conceptual point of view, optimal detection of LoRa signals can be performed through the following maximum *a posteriori* probability (MAP) detection strategy [4]:[2]

$$\hat{a}_0 = \underset{a_0}{\operatorname{argmax}}\, \Re\{z(a_0)\} \tag{9}$$

having defined

$$z(a_0) = \int_{-T/2}^{T/2} r(t)\xi^*(t; a_0)\, dt$$

i.e., $z(a_0)$ is obtained by sampling the received signal $r(t)$ filtered through a filter matched to $\xi(t; a_0)$. We can thus conclude that a sufficient statistic can be obtained through a bank of $N = 2^{\mathrm{SF}}$ filters matched to all possible waveforms $\xi(t; a_0)$.

Although this receiver is quite simple from a conceptual point of view, it can hardly be implemented when N grows.

[2]This detection strategy has been obtained by exploiting the fact that $\xi(t; a_0)$ has a constant envelope.

Let us consider a digital implementation of the bank of N matched filters. In practical receivers, an approximated set of sufficient statistics is obtained through the technique described in [5]. It is assumed that the LoRa low-pass equivalent is band limited with bandwidth $B/2$—although this is not strictly true as discussed in the previous section. The approximated statistics can be obtained by sampling the received signal prefiltered by means of an ideal analog low-pass filter having bandwidth $B/2$.

The use of an ideal filter ensures that the noise samples are i.i.d. complex Gaussian random variables with independent components. As discussed in the previous section, we need at least N samples to represent the transmitted signal in the interval $[-T/2, T/2]$. The complexity related to the implementation of N matched filters is thus proportional to N^2.

A significant complexity reduction can be obtained by exploiting (8). In fact, we can express the received samples as

$$r_n = \xi_n(a_0 = 0)e^{-j\frac{2\pi}{N}a_0 n} + w_n$$

where w_n are AWGN samples [5]. We can thus remove the up-chirp signal by computing

$$y_n = r_n^* \xi_n(a_0 = 0) = e^{j\frac{2\pi}{N}a_0 n} + w_n'$$

where w_n' are still AWGN samples since the up-chirp signal has a constant amplitude and does not modify the noise statistics. The optimal MAP detection strategy based on these samples can be expressed as

$$\hat{a}_0 = \underset{a_0}{\operatorname{argmax}}\, \Re\left\{\sum_{n=0}^{N-1} y_n e^{-j\frac{2\pi}{N}a_0 n}\right\}. \tag{10}$$

Looking at (10), we can recognize that the strategy can be expressed as

$$\hat{a}_0 = \underset{k}{\operatorname{argmax}}\, \Re\{Y_k\}$$

having defined

$$Y_k = \sum_{n=0}^{N-1} y_n e^{-j\frac{2\pi}{N}kn}$$

as the discrete Fourier transform (DFT) of samples y_n. It can be thus efficiently computed through the fast Fourier transform (FFT) with complexity $N \log_2 N = N \cdot \mathrm{SF}$.

The error probability of strategy (10) is known in an analytic form. In fact, since the discrete-time waveforms are orthogonal, the symbol error probability is exactly the same as that of any other orthogonal modulation scheme [4].

As said, strategies (9) and (10) are only approximately equivalent. In fact, strategy (10) has been obtained under the approximated assumption that LoRa signal (1) has a limited bandwidth $B/2$. Although not strictly true, we found that the performance loss in terms of symbol error rate is negligible (less than 0.01 dB) with respect the optimal receiver, for the SF of interest, e.g., $7 \leq \mathrm{SF} \leq 12$. We can conclude that the approximation that allows to obtain strategy (10) is very good.

B. Noncoherent Detection

Detection strategies (9) and (10) have been obtained under the assumption of ideal synchronization. We will now consider phase noise and the related performance loss it produces on strategies (9) and (10).

The optimal detection strategy in the presence of phase noise will depend on the channel coherence time. When the channel coherence time is long enough, we can exploit its correlation to design a receiver with a memory having negligible performance loss with respect to the case of ideal synchronization [6]. On the other hand, when the channel phase is assumed to change independently every symbol interval, the system is again memoryless and the receiver will have the lowest possible complexity. It can be easily shown that when the channel phase is assumed to be uniformly distributed and to change independently every symbol interval, the strategies (9) and (10) become [4]

$$\hat{a}_0 = \underset{a_0}{\operatorname{argmax}} |z(a_0)| \tag{11}$$

and

$$\hat{a}_0 = \underset{a_0}{\operatorname{argmax}} \left| \sum_{n=0}^{N-1} y_n e^{-j\frac{2\pi}{N} a_0 n} \right|. \tag{12}$$

These kinds of strategies are called "noncoherent" in the literature. In particular, we will consider strategy (12) only, since it can be implemented through the FFT. Its error probability is known in analytical form [4]. The performance loss with respect to coherent detection is lower than 0.5 dB. Thus, it is not worth investigating the possibility to exploit the phase–noise correlation in case of a longer coherence time.

C. Properties of LoRa Signals to be Exploited for Synchronization

In this section, we will discuss the synchronization of LoRa signals. In particular, we will see which properties of LoRa signals can be exploited to perform frame, frequency, and timing synchronization. In Section III-H, we will describe the entire synchronization procedure.

The preamble of a LoRa packet is characterized by eight consecutive up-chirps, two "special" known modulated symbols, and 2.25 down-chirps [7], where the down-chirp is just the complex conjugate of the up-chirp. Let us consider an up-chirp signal in the reference interval $[-T/2, T/2]$. It can be expressed in closed form as [see (7)]

$$\begin{aligned}\xi(t;0) &= \sqrt{\frac{2E_s}{T}} \exp\left\{ j2\pi B \int_{kT-T/2}^{t} \Gamma(\tau;0)\, d\tau \right\} \\ &= \sqrt{\frac{2E_s}{T}} \exp\left\{ j2\pi B \left(\frac{t^2}{2T} - \frac{T}{8} \right) \right\}.\end{aligned}$$

Let us now assume that a train of up-chirp signals experiences a delay τ (we will assume $0 \le \tau \le T$) and is affected by a frequency uncertainty ν (due to the uncertainty on the nominal frequency of the transmitted signal and the Doppler shift related to the satellite motion) and a phase shift θ_0, in addition to the AWGN.[3] The complex envelope of the received signal can be thus expressed as

$$r(t) = \beta \sum_k \xi(t - kT - \tau; 0) e^{j(2\pi\nu t + \theta_0)} + w(t)$$

where β is the attenuation due to propagation and $w(t)$ is the complex Gaussian AWGN process.

Due to the presence of the frequency uncertainty ν, a discrete-time sufficient statistic can still be obtained with the same technique already described in Section III-A, but N samples per symbol are no more sufficient. We will thus need to extract N_o samples, with $N_o > N$, after the analog prefilter. These samples $\{r_n\}$ are then multiplied by the complex conjugate of the samples of the original train of up-chirp signals (dechirping operation). Without loss of generality, we will assume that the sequence used for this dechirping operation has a unit amplitude. This multiplication does not change the noise statistics. The received samples after dechirping in the reference symbol interval $[-T/2, T/2]$ can be expressed as

$$y_n = s_n + w_n\,, \quad n = -\frac{N_o}{2}, -\frac{N_o}{2} + 1, \ldots, \frac{N_o}{2} - 1 \tag{13}$$

where w_n is a discrete-time complex white Gaussian noise process and samples s_n can be expressed as

$$s_n = \begin{cases} \gamma e^{j\theta_1} e^{j2\pi\left(B+\nu-B\frac{\tau}{T}\right)n\frac{T}{N_o}} & -\frac{N_o}{2} \le n < -\frac{N_o}{2} + N_1 \\ \gamma e^{j\theta_2} e^{j2\pi\left(\nu-B\frac{\tau}{T}\right)n\frac{T}{N_o}} & -\frac{N_o}{2} + N_1 \le n < \frac{N_o}{2} \end{cases}$$

where γ is a proper amplitude, taking into account the amplitude of the transmitted signal and the channel attenuation and having defined $N_1 = \lfloor N_o \frac{\tau}{T} \rfloor$, where $\lfloor x \rfloor$ denotes the largest integer lower than or equal to x, and

$$\theta_1 = 2\pi B \left(\frac{T}{2} + \frac{\tau^2}{2T} - \tau \right) + \theta_0$$

$$\theta_2 = 2\pi B \frac{\tau^2}{2T} + \theta_0.$$

The computation of the Fourier transform of sequence s_n, $n = -\frac{N_o}{2}, -\frac{N_o}{2} + 1, \ldots, \frac{N_o}{2} - 1$, will exhibit a maximum of amplitude $\gamma \cdot \max(N_1, N_o - N_1)$ either at frequency $(\nu - B\frac{\tau}{T})$ or at frequency $(B + \nu - B\frac{\tau}{T})$, depending on the value of N_1. This maximum can be identified by using the Rife and Boorstyn algorithm [8] which is based on two steps. A *coarse search* is first performed by computing some samples of the Fourier transform through the FFT and looking for the maximum sample. An interpolation is then performed around this maximum sample to refine the search (*fine search* step).

If we repeat the same operations for the down-chirp signal (this time using the down-chirp signal to perform dechirping) we obtain again a maximum of amplitude $\gamma \cdot \max(N_1, N_o - N_1)$ but this time either at frequency $(\nu + B\frac{\tau}{T})$ or at frequency $(B + \nu + B\frac{\tau}{T})$. In the next sections

[3] We will consider the effect of the Doppler rate α later.

we will see how to exploit this property to perform frame, frequency, and timing estimation.

When a Doppler rate α is also present, we observe an uncompensated frequency offset ν that varies linearly with time at a slope α. In order to qualitatively understand the effect of this Doppler rate, let us approximate this linear variation with a staircase, i.e., constant over a symbol and changing from symbol to symbol. Under this assumption, the frequency corresponding to the maximum amplitude of the Fourier transform, when performed on consecutive symbols, will increase or decrease linearly (depending on the sign of α). We have to take this into account when performing synchronization and detection.

D. Estimation of the Frequency Peaks

The estimation of the above-mentioned frequency peaks is a challenging task. In fact, in typical operating conditions the energy of a single sample is far lower than the noise power, leading to a high number of outliers in the estimation process that could degrade the performance. Because of this, algorithms for frequency estimation working in the time domain, such as that by Mengali and Morelli [9] which has, for high signal-to-noise ratio (SNR) values, a performance close to that of the Rife and Boorstyn algorithm but with a lower complexity, become useless since they start converging only at very high SNR values.

A simple approach to reduce the occurrence of the outliers is the following: instead of considering the FFT of a block of samples related to a single symbol, we compute the magnitude of the transform of two symbols and sum them together. In this way, peaks due to noise are averaged out and signal peaks will sum constructively. The fine estimation is made through zero-padding before FFT. As shown later, this is not an optimal approach since the estimator's performance is farther from the MCRLB but convergence is reached at lower SNR values.

A similar procedure for computing the magnitude of the transform of more symbols and summing them together can also be employed when searching for the preamble to perform frame synchronization. The difference is that at this stage the receiver does not need the fine estimation step since we are only interested in revealing the presence of the preamble pattern.

E. Frame Synchronization

The first step in the synchronization procedure is the detection of the presence of a transmitted packet through the search of the known preamble. We will say that the receiver is in *listen mode*. A *coarse search* for the preamble must be performed either continuously or at given time intervals, depending on the working procedure agreed by the gateway and user terminals. We will assume a continuous operation mode. The search is performed by considering blocks of nonoverlapping N_o samples, removing the up-chirp from them (dechirping operation), processing them through FFT, and summing the magnitude of the FFTs of two consecutive blocks. Now we can look for the maximum value of this sum of magnitude of the computed FFTs. Then, we move forward one symbol and repeat the operation. In practice, pairs of blocks are considered, with an overlap of one block between two consecutive pairs. When the maximum of the FFTs of seven pairs of blocks of symbols are all in the same position on the FFT grid despite the values of the frequency and timing offsets, we are in the presence of eight up-chirps.

As discussed in the previous section, two peaks at a distance of B can be observed. When $N_1 \simeq N_o/2$, these two peaks will have similar amplitudes and, in the presence of noise, the maximum FFT value can be one of them. So it can happen that from a symbol to the next, the position of the maximum can have a "jump" of B. Moreover, it can happen that a specific value of the fractional delay and the presence of a significant Doppler rate lead to peaks which can shift up to ± 2 samples of the Fourier transform from the beginning to the end of the preamble up-chirps. Hence, proper control procedures must be envisaged to take into account all these effects when searching for the preamble. In other words, we do not have to look for seven consecutive peaks at the same frequency sample but we have to relax this constraint by looking for less than seven consecutive peaks and possibly not exactly at the same frequency—the number of peaks to be searched has to be defined with proper simulations aimed at finding a good compromise between missed detection probability (that will increase the packet error rate) and the false alarm probability.[4] An increase in the false alarm probability is not a problem per se. In fact, even if we erroneously identify a preamble, the verification of the cyclic redundancy check (CRC) after detection will allow to correctly identify the absence of a valid packet. It is, however, important that the receiver remains in listen mode even when it believes that a preamble has been identified. This will cost a slight increase in the computational complexity but will prevent that a valid packet is lost when the receiver leaves the listen mode to start detecting the payload. In any case, this has to be made if we want to simultaneously detect interfering packets.

The previous step is able to identify the presence of a packet but, due to the relaxed constraints we adopted, we will have a significant uncertainty on the beginning of a packet. As a consequence, the receiver has to start a *fine-frame synchronization procedure*. The aim of this procedure is to confirm the presence of a packet, to identify its position more precisely, and to reduce the uncertainty on the timing offset. This time, we take blocks of ten consecutive symbols. For eight of them, dechirping is performed as usual whereas, for the last two, dechirping is performed by multiplying them for the complex conjugate of the two "special" known symbols in the preamble. The magnitude of the FFTs of these ten symbols are computed, then summed, and

[4]By only considering the missed detection probability, which is the most critical one, we found that we have to search for four peaks with a tolerance in the position of ± 2 FFT samples.

both position P and amplitude A of the maximum of the result are computed and stored. The window containing these ten symbols is then shifted $T/4$ and the same operations are performed over another block of ten symbols, partially overlapped with the previous one. When all possible positions compliant with the uncertainty of the previous step have been tested, we keep that corresponding to the largest stored value of the amplitude A. In this case, the starting position of a packet is identified with an uncertainty lower than $T/4$.

F. Timing and Frequency Synchronization

After frame synchronization, timing and frequency can be estimated. We will see later in Section III-H that this task has to be performed in two steps (a coarse and a fine one) with Doppler rate estimation and a tight filtering in the middle. In both steps the procedure is the same.

The position P of the peak obtained in the fine-frame synchronization step will provide an estimate of either the frequency $\left(\nu - B\frac{\tau}{T}\right)$ or the frequency $\left(B + \nu - B\frac{\tau}{T}\right)$. By repeating the same operation on the two down-chirp symbols we will obtain an estimate of either the frequency $\left(\nu + B\frac{\tau}{T}\right)$ or the frequency $\left(B + \nu + B\frac{\tau}{T}\right)$. We now have to extract an estimate of both ν and τ. Then, it should be considered that an ambiguity arises in the derivation of the frequency and timing offset contributions, due to the fact that we have two possible values of the position of the largest peak (as an example, on the up-chirp symbols we do not know if we identified the peak at frequency $\left(\nu - B\frac{\tau}{T}\right)$ or that at frequency $\left(B + \nu - B\frac{\tau}{T}\right)$) and to the cyclic nature of the FFT. We thus have to disambiguate different pairs of values of frequency and timing offsets from each pair of estimated tones. Some of them will correspond to values of either the timing offset or the frequency uncertainty outside the allowed ranges. The remaining pairs can be disambiguated through a trial-and-error procedure that consists in applying the compensation pair to an up-chirp block and then verifying if the maximum of its FFT is located in the zero (the continuous component or direct current, dc) tone (it is worth noting that it is not necessary to perform a whole FFT processing on the symbol, but rather a processing on the tones around dc only, since this is a disambiguation procedure so that only in one case the dc tone will be clearly recognizable).

G. Doppler Rate Estimation

The frequency shift due to the Doppler effect has to be cumulated with that coming from the frequency instability of the employed oscillators, and can be estimated as described in the previous section. On the contrary, the Doppler frequency shift variation, i.e., the Doppler rate, is peculiar of the satellite link scenario. The main problem here is that, essentially, the LoRa modulation was not designed to deal with it. The maximum value of the Doppler rate, for a typical altitude of 650 km of a LEO satellite and given the carrier frequency of the LoRa signals (which in the worst case corresponds to 928 MHz [10]), is of 245 Hz/s (see [11]).[5] The Doppler rate entails a frequency deviation, from one symbol to the next, which is comparable to the frequency separation between two adjacent symbols, for the highest values of SF. In fact, for SF $= 12$ the separation is approximately 30 Hz (for SF $= 11$, it is approximately 61 Hz). Since the frequency variation due to the Doppler rate from one received symbol to the next can be up to 8 Hz, this means that, for SF $= 12$, the symbol sequence can be shifted by one position every four received symbols.

In the presence of Doppler rate, the received samples (13) become

$$z_n = s_n \exp\{j2\pi\alpha k^2 T_s^2\} + w_n \tag{14}$$

where α represents the Doppler rate and $T_s = T/N_o$ the sampling time. The system sensitivity to Doppler rate can be evaluated through simulations. We considered the cases SF $= 10$ and 12 and packets of 45 symbols without preamble, and computed the packet error rate (PER) versus the signal-to-noise ratio for different values of the uncompensated Doppler rate. The results, not reported here due to a lack of space, state that for SF $= 12$, a significant penalty is already observed for a Doppler rate around 6 Hz/s, whereas the PER is equal to one when the Doppler rate exceeds 10 Hz/s. In fact, simple calculations show that, in this case, a Doppler rate of 11 Hz/s yields a symbol shift by the end of the packet, even in the absence of noise. Hence, it is required to estimate the Doppler rate value with an accuracy of a few Hz/s. In the case of SF $= 10$ instead, higher values of Doppler rate are required to worsen the performance. As an example, a value of α larger than 150 Hz/s is required to give a PER of one.

Several algorithms for data-aided (DA) Doppler rate estimation exist. One of the most effective algorithms is that proposed in [12], and can be directly applied to the received signal once modulation and chirping have been removed, and timing and frequency offsets have been compensated for. However, when applied to the available preamble in our scenario, again we observe that convergence is reached for high values of the SNR only. In addition, all these algorithms result to be unreliable under nonideal conditions, since the phase jumps between adjacent symbols, due to imperfect timing compensation, severely affect their performance.

We thus considered an algorithm based on the Rife–Boorstyn technique used to obtain the estimates of the peak position on each symbol interval, and on the processing of different estimates. The peak frequency values are processed in order to find the linear regression which represents the frequency slope due to Doppler rate. Nevertheless, the few available data suffer again by a high incidence of outliers, which are partly due to the low SNR, but also due

[5] [11, Eq. (5)] provides the general expression of the Doppler shift for a satellite, given its speed and angular position. Its time derivative yields the Doppler rate expression.

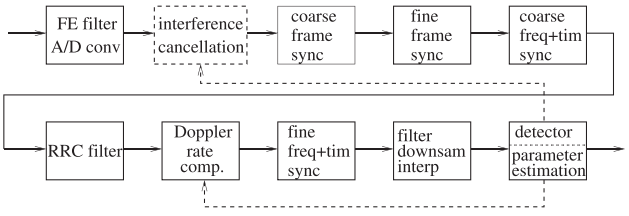

Fig. 3. Overall receiver.

to the residual timing error. We thus propose the algorithm summarized by the following steps.

1) Nine out of 12.25 preamble symbols (the first one and the 2.25 down-chirps are rejected[6]) are used for a first iteration Doppler rate estimate.
2) We compute the nine frequency estimates ν_i, one for each known symbol. Those with $|\nu_i| > 4/T$ are considered as outliers and purged. In fact, Doppler rate estimation is performed after the coarse frequency synchronization step. Thus, the expected values of ν_i must be around zero if we except the deviation caused by the Doppler rate. We are here admitting that the Doppler rate can, at most, move the peak in frequency of four FFT samples.
3) The remaining frequencies are used in pairs to compute different Doppler rate estimates, by exploiting each possible combination of ν_i pairs—the Doppler rate estimates are computed as $(\nu_i - \nu_j)/\Delta_{|i-j|}$, where $\Delta_{|i-j|}$ represents the frequency separation between peaks.
4) An average over all the estimates is then performed, and if the estimate $\hat{\alpha}$ is out of the expected range (i.e., $|\hat{\alpha}| > 245$ Hz/s for the mentioned typical altitude of 650 km), the estimated Doppler rate is set to zero to avoid deteriorating the processed signal.
5) The estimated Doppler rate is finally removed from the signal.

Essentially, the average over these two-point linear regressions turns out to have a better performance than computing a single linear regression estimate using all symbols, since the effect of the outliers is more likely to be averaged out. The performance of the proposed algorithm will be assessed in Section V.

H. Overall Receiver

The overall receiver, comprising the synchronization and detection procedure, is shown in Fig. 3.

1) As previously mentioned, the received analog signal is first filtered through a front-end prefilter and then sampled at frequency $F_s = \frac{N_o}{T} \geq B + 2\nu_{\max}$, where $\nu_{\max}$ is the maximum value of the frequency uncertainty, which can be readily found to be equal to $B/2$ for the case $N_o = 2N$. Considering the value of $\nu_{\max}$ for a LEO satellite, the bandwidth of the analog prefilter will be much larger than that of the transmitted signal (and we will also need to sample with $N_o \simeq 2N$ samples). A large amount of noise will thus affect the received samples and this will have an impact on the performance of the synchronization algorithms that have to be performed in two steps (a coarse and a fine one), as discussed in the following.
2) After sampling, the contribution of a previously detected packet is removed, if interference cancellation is envisaged (see Section III-I).
3) Coarse and fine frame synchronization, as described in Section III-E, will then take place.
4) We can now perform coarse frequency and timing estimation as described in Section III-F.
5) After the coarse compensation of timing and frequency offset, a tight filtering can be performed in order to reduce the excess noise and improve the performance of the following estimation steps. We used a filter with root-raised cosine (RRC) amplitude and linear phase, with roll-off factor 0.06 (optimized through simulations) and bandwidth B.
6) At this stage, the Doppler rate estimation and compensation is performed, for the modulation formats corresponding to the higher SF values only (for lower SF values, this step is not required since the performance loss entailed even by the maximum Doppler rate value is negligible). The employed algorithm is based on processing the position of the frequency peaks of the up-chirp symbols and of the "special" known symbols in the preamble (nine symbols overall), as previously described.
7) Fine frequency and timing estimation is then performed. The algorithm is exactly the same used in the coarse step, but this time we take advantage of the suppression of the excess noise and of the Doppler rate compensation. After the estimation, the frequency shift is compensated. Regarding the estimated timing, the integer part, corresponding to an integer number of samples, is easily performed.
8) Fractional timing compensation and downsampling to N samples can now take place at the same time, through interpolation.
9) Noncoherent detection is finally performed.
10) The accuracy of the Doppler rate estimate should allow the detection of a first bunch of payload symbols, which in turn can be used to refine the estimate, thus increasing the accuracy. However, after a first Doppler rate compensation, the frequency and timing estimation procedure must be repeated. In other words, detected symbols are used to refine the Doppler rate estimation and the fine and frequency estimation, so we come back to step 6, by employing a limited number of detected symbols

[6]The down-chirps cannot be used because the unavoidable imperfect timing compensation leads to a phase shift with respect to the up-chirped symbols, which typically worsen the final estimate.

TABLE I
Data Rates Allowed by LoRaWAN for the LoRa Signals

Region	Bandwith [kHz]	Approx. data rate [bps] (SF)	r_c
EU, CN	125	250 (12), 440 (11)	4/6
EU, CN, US, AU		980 (10), 1760 (9), 3125 (8), 5470 (7)	4/5
EU, CN	250	11000 (7)	4/5
US, AU	500	980 (12) , 1760 (11)	4/6
		3900 (10), 7000 (9), 12500 (8), 21900 (7)	4/5

at each subsequent feedback, until the end of the transmitted packet is reached.

I. Interference Cancellation

In the case of packet collisions, interference cancellation can still allow to detect the transmitted packets. We will consider hard interference cancellation only, where already detected packets are canceled from the received signal in the attempt to detect the underlying packets with lower power.

In order to perform interference cancellation, we have to estimate, in addition to the Doppler rate, the Doppler shift and the timing, also the signal amplitude and the signal phase. Although we already have an estimate of Doppler rate, Doppler shift, and timing, the accuracy could be not sufficient to perform a suitable cancellation.[7] To understand this aspect, we performed some preliminary simulations to evaluate the amount of amplitude reduction of the detected signal we have to achieve in order to have some benefit in the overall performance. We found that it is sufficient to have a reduction of 60%–80% of the amplitude of the detected signal from the received one to have a significant benefit. On the other hand, the further benefits entailed by a reduction of 90% is very limited. As a consequence, we decided to use, in the cancellation step, the estimates of Doppler rate, Doppler shift, and timing already obtained before detection. We thus only performed amplitude and phase estimate. Since a remodulated copy of the transmitted packet is available, the time-varying channel phase is estimated using the DA version of the Tikhonov algorithm proposed in [13]. After that, the time-invariant amplitude is computed following the procedure explained in [14]. The last step of the interference cancellation is the subtraction of the reconstructed waveform from the received signal.

IV. SYSTEM SIMULATOR

In order to provide more comprehensive results on the performance of the proposed receiver and on the suitability of a LEO reception for LoRa signals, a system simulator was conceived and designed, accounting for all the relevant parameters that can be found in a realistic scenario. We included the main features of the LoRaWAN network protocol that can be summarized as follows. Given the scenario, we privileged high SF that entail low data rates (the allowed range is $0.3 \div 50$ kbps), uplink traffic (from CT to the satellite), class A devices (see [10] for details), all available frequency slots, guard bands of 75 kHz (the frequency uncertainty can be up to ± 50 kHz), the standard message structure (a preamble with 8 up-chirps, followed by 2 shifted up-chirps, and 2.25 down-chirps), a fixed-length payload, and the CRC. For the sake of simplicity, we assumed that the simulated receiver is aware of the packet lengths, without simulating the header (i.e., the LoRa physical header protected by its own CRC, containing information on the transmitted message), since this choice does not affect the performance. The radiated power is given in terms of equivalent isotropic radiated power (EIRP). The allowed values in Europe are 2, 5, 8, 11, 14 dBm. Table I reports the possible employed values of the code rate r_c[8] in the different regions—Europe (EU), United States (US), China (CN), and Australia (AU), according to [10].

In the described network, a given number of packets following the LoRaWAN standard and transmitted to the satellite will be simulated. The designed receiver tries to detect as many transmitted messages as possible, through successive detection and cancellation, and computes the number of correctly detected messages. Given the users' density, the aim of the simulator is to derive:

1) the percentage of correctly received packets per SF and in total;
2) the percentage of users whose transmitted packet is correctly decoded in at least one of the retransmissions (which can happen with different values of SF).

We assume that all users are uniformly distributed within the field of view (FoV) of the satellite. Each CT transmits at the maximum allowed value of EIRP, which depends on the region of interest. Moreover, the data rate values also depend on the considered region and on the SF chosen for the packet transmission. In the FoV, different areas (rural, urban, etc.) can be uniformly present. The number of transmitted packets is N_{p}, and the satellite will receive only a fraction of it.

The N_{u} CTs are assumed to be uniformly distributed within the FoV of the satellite. Each CT can retransmit his packet once ($N_{\mathrm{rep}} = 1$), or not ($N_{\mathrm{rep}} = 0$), so that the

[7] Obviously, the cancellation will never be perfect, but we will only obtain a reduction of the amplitude of the detected signal from the received one.

[8] We were not able to find the description of the codes employed in the LoRaWAN protocol, but only the corresponding rates. For this reason, we simulated uncoded transmissions as they represent a worst case.

relation $N_p = N_u(1 + N_{rep})$ holds. Due to the random access, there is a probability that packets of two or more users collide. Considering that with the bandwidth values at stake (at most 500 kHz), the channel is frequency flat, the model for the complex envelope of the received signal at the LEO satellite is thus

$$r(t) = e^{j\theta(t)} \sum_{i=1}^{N_p} \gamma_i(t) s_i(t - \tau_i) \exp\left\{2\pi \nu_i t + 2\pi t \int_0^t \alpha_i(\tau) d\tau + \phi_i(t)\right\} + w(t) \quad (15)$$

where:

1) $s_i(t - \tau_i)$ is the message transmitted by the ith active user. LoRa modulation has a complex envelope and a continuous phase. As a consequence, there is no need to take into account the nonlinear distortions of the transmit amplifier;
2) $\gamma_i(t)$ is its gain/attenuation introduced by the channel. On a fading channel, this coefficient is complex and possibly time varying. Since the main reason for time selectivity is related to the satellite speed, we neglect the very limited impact of the CT mobility. In addition, from simple geometric considerations it is possible to demonstrate that, even in the worst case, the angular position of the satellite has a very limited change during the duration of a packet. Hence, we can assume the channel to be static apart from the presence of the uncompensated frequency offset, the Doppler rate (taken into account separately), and the phase noise. Coefficients $\{\gamma_i\}$ can be thus considered as time invariant for the whole packet duration;
3) ν_i is the uncompensated frequency offset of signal $s_i(t)$. It takes into account the Doppler shift and the frequency instability of the transmit oscillator only (± 30 parts per million (ppm), which corresponds to, approximately, ± 30 kHz) since the receive oscillator is assumed much more stable;
4) α_i is the Doppler rate;
5) $\theta(t)$ the receiver phase noise;
6) $\phi_i(t)$ the phase noise at the ith transmitter, assumed independent of the receiver phase noise;
7) τ_i is the relative delay of the ith packet;
8) $w(t)$ is the AWGN.

Coefficients γ_i take into account the radiation patterns of the employed antennas, path losses (Friis transmission equation), and other channel propagation effects. Since the antenna gain depends on the elevation angle and the receive power depends on the distance between the antennas, these gains are influenced by the users' positions, that were taken into account in the system simulator. For the specific channel we are considering, we believe that free space path attenuation is a good model so we neglected advanced models that describe signal propagation in urban areas (attenuation as a function of the mth power of the distance between antennas).

Then, we also took into account the presence of CTs in urban areas that can be subject to shadowing. Given the low values of transmitting power, the probability that a signal transmitted by one of such terminals can be received by the satellite is very low. We thus considered a shadowing model described by the Bernoulli distribution, defined by a probability p, which reduces the user density by a factor p. All CTs in rural areas are assumed to be in line of sight with the satellite, otherwise their packets will hardly be detected by a receiver on board a LEO satellite. Their corresponding coefficients γ_i can be thus modeled as Ricean distributed. Parameter K of this Ricean distribution will be different for different CTs since it will depend on the reflectors around them. So this parameter needs to be properly modeled. However, let us consider a given CT and assume that we know the corresponding Ricean parameter. We could randomly generate the value of γ_i according to this distribution but the corresponding random fluctuation that we will have is equivalent to move the CT to another location. Considering that we randomly generate the positions of the CTs and the results we show are averaged over many different positions, the performance we obtain will not be affected by the choice we make on the model for Ricean parameter.

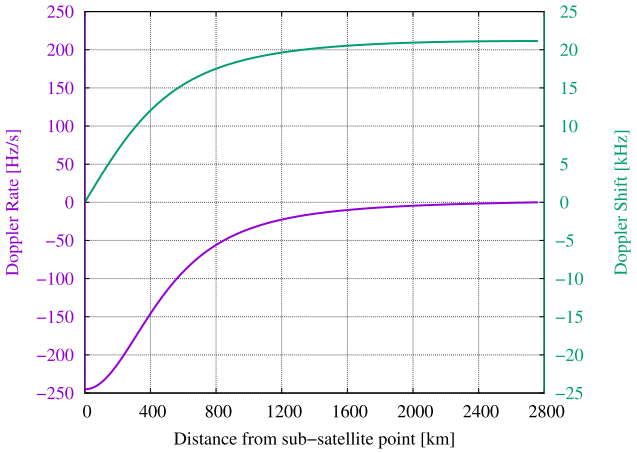

Fig. 4. Doppler shift (upper curve) and Doppler rate (lower curve) values for a LEO satellite flown over the Australian region.

An extra attenuation was also taken into account, to allow a conservative link budget design. Some margins were taken into account for miscellaneous losses, for example:

1) a 3 dB polarization mismatch;
2) a 0.3 dB atmospheric losses due to rain, cloud, or O_2 absorption since the frequency bands defined in LoRaWAN protocol are within the subGHz spectrum [15], [16].

Regarding Doppler effects, in Fig. 4 we report the Doppler shift and the Doppler rate as a function of the distance between subsatellite point and the CT. It can be noticed that the maximum values correspond to $|\nu| \simeq 21.15$ kHz and $|\alpha| \simeq 245$ Hz/s, respectively.

We assumed that the CT is equipped with a quarter-wave monopole, one of the most employed low-cost antennas used in IoT applications thanks to its omnidirectionality [17]. This antenna has a null in the azimuthal direction. In our simulator, for each CT the azimuthal direction was selected randomly. The satellite has an 8-turn helical

TABLE II
Values of C/N Required to Achieve a BER $= 10^{-5}$ Over AWGN Channel, Uncoded Transmission, and No Interfering Signals

SF	7	8	9	10	11	12
C/N **[dBW]**	-6.9	-9.7	-12.5	-15.3	-18.1	-20.9

antenna with diameter 10.5 cm, and tilt 55 degrees. The corresponding gain is 12.4 dB [17].

Let P_{TX} be the power transmitted by the user terminal that depends on the considered region, L the line-of-sight path loss, G_{TX} the transmitter antenna gain, G_{RX} the receiver antenna gain, $k_{\mathrm{B}} = 1.38 \cdot 10^{-23}$ J/K the Boltzmann constant, T_{N} (450 K in our simulations) the equivalent noise temperature, and L_{M} the miscellaneous losses (which we took equal to 3.3 dB to account for polarization mismatch and atmospheric losses, as previously stated). It is possible to express the ratio C/N seen by the satellite by using the Friis formula as

$$\left.\frac{C}{N}\right|_{\mathrm{dB}} = \left.P_{\mathrm{TX}}\right|_{\mathrm{dBm}} + \left.L\right|_{\mathrm{dB}} + \left.G_{\mathrm{TX}}\right|_{\mathrm{dB}} + \left.G_{\mathrm{Rx}}\right|_{\mathrm{dB}} - 10\log_{10}(k_{\mathrm{B}}T_{\mathrm{N}}B) + \left.L_{\mathrm{M}}\right|_{\mathrm{dB}}. \quad (16)$$

The path loss is simply

$$\left.L\right|_{\mathrm{dB}} = 20\log_{10}\left(\frac{\lambda}{2\pi}\right) - 20\log_{10}(R_{\mathrm{u}})$$

where λ is the wavelength based on the selected channel and R_{u} is the distance between the user and the satellite, according to the CT's position in the FoV.

Once C/N is known, it is possible to compute the ratio E_{s}/N_0 as

$$\left.\frac{E_{\mathrm{s}}}{N_0}\right|_{\mathrm{dB}} = \left.\frac{C}{N}\right|_{\mathrm{dB}} + 10\log_{10}\left(2^{SF}\right).$$

The ratio E_{b}/N_0, where E_{b} is the mean energy per bit, can be expressed as

$$\left.\frac{E_{\mathrm{b}}}{N_0}\right|_{\mathrm{dB}} = \left.\frac{C}{N}\right|_{\mathrm{dB}} + 10\log_{10}\left(\frac{2^{SF}}{SF}\right) - 10\log_{10}r_{\mathrm{c}} = \left.\frac{E_{\mathrm{s}}}{N_0}\right|_{\mathrm{dB}} - 10\log_{10}(SF) - 10\log_{10}r_{\mathrm{c}}$$

where r_{c} is the forward error correction (FEC) code rate.

Let us now make some considerations on the closure of the link budget. As mentioned, for a LoRa signal there is a closed-form expression of the bit error rate (BER) versus E_{b}/N_0. Considering that E_{b}/N_0 is related to the C/N, as seen in (17), for a BER of 10^{-5} the corresponding CNR values are shown in Table II. If these values are compared to the link budget of a typical EU scenario, it can be concluded that not all values of the spreading factor can achieve the target BER. Moreover, it has to be considered that our scenario is *interference limited and not thermal noise limited*, so the set of available parameters will be further restricted. Reasonably, it is expected that only LoRa signals with high values of SF can be decoded.

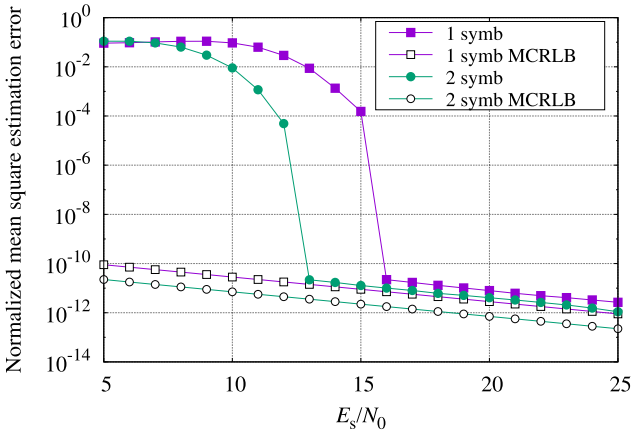

Fig. 5. Normalized MSEE for the adopted algorithms used for the identification of the frequency peaks. The corresponding MCRLB is also reported for comparison.

We expect that the CTs employ very cheap oscillators whereas we may assume that the oscillator at the satellite has much better characteristics. For this reason, we will only consider the transmit phase noise. According to the phase-noise mask in [18], a proper phase-noise model can be derived, but in the system simulator we did not use it. In fact, we decided to implement a more challenging phase noise based on the Wiener model whose parameter has the minimum value such that the implemented Wiener phase-noise mask is always above that in [18].

V. NUMERICAL RESULTS

In this section, we will first assess the performance of the proposed receiver in the presence of Doppler shift and Doppler rate through computer simulations. We consider here the case of a simple AWGN channel in the absence of interference—performance in a more realistic scenario where interference also takes place is considered in system simulations.

A. Synchronization Algorithms

1) *Frequency Peak Estimation:* We investigated the convergence properties of the Rife and Boorstyn algorithm. In Fig. 5, we report the mean-square estimation error (MSEE), normalized to N_{o}/NT, versus E_{s}/N_0 for the Rife and Boorstyn algorithm applied to the samples of a single symbol (thus to a total number of samples N_{o}) for the case with SF $= 12$. Results refer to the algorithm considering the FFT of a block of samples related to a single symbol and that computing the magnitude of the transform of two symbols summed together, as explained in Section III-D. We chose $N_{\mathrm{o}} = 2N$ for the reasons explained previously. It can be observed that, in both cases, the performance approaches the modified Cramér–Rao lower bound (MCRLB) [19], also reported for convenience, for high values of E_{s}/N_0 only. For lower values, a significant number of outliers is observed. These outliers degrade the performance. The sum of the magnitude of the transforms of two symbols allow to

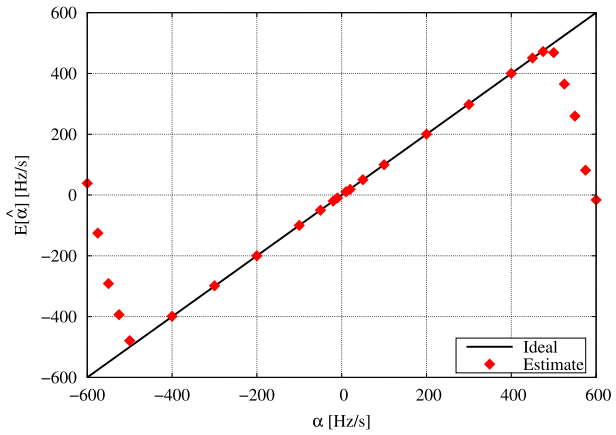

Fig. 6. Average value of the Doppler rate estimate for SNR = 20 dB.

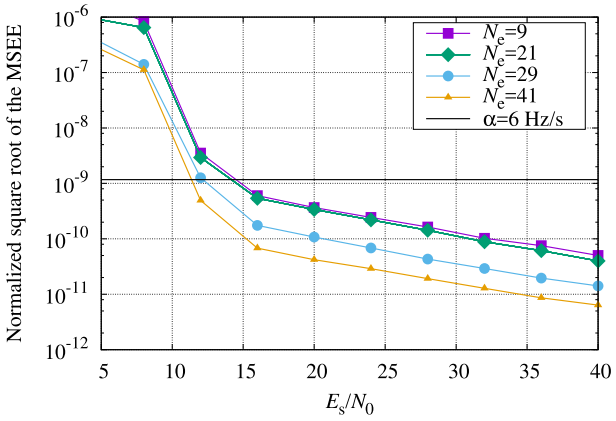

Fig. 7. Normalized square root of the MSEE for increasing number of employed symbols.

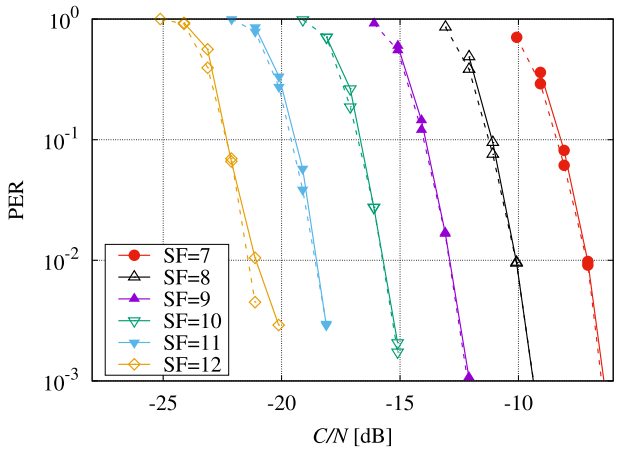

Fig. 8. PER performance of the designed receiver in the presence of Doppler shift and Doppler rate (continuous lines), and with perfect estimation and compensation (dashed lines), for $7 \leq \mathrm{SF} \leq 12$.

reduce the threshold above which the algorithm approaches the bound.

We now consider the estimation of the Doppler rate. Fig. 6 shows the mean value, obtained by averaging over 1000 trials per point, of the estimated Doppler rate $E[\hat{\alpha}]$ as a function of the true value, for an SNR of 20 dB and $\mathrm{SF} = 2$, and assuming perfect timing and frequency offset compensation. It can be seen that the proposed algorithm is unbiased in a range which is much larger than that corresponding to the values of the Doppler spread corresponding to a LEO satellite with altitude 650 km.

The performance of the algorithm is then assessed and shown in Fig. 7 in terms of the square root of the MSEE, normalized to the sampling frequency, obtained by averaging over 10 000 trials per SNR value, again assuming perfect timing and frequency offset compensation. The required minimum value of the accuracy (6 Hz/s, which was previously identified as a critical value) is also reported for comparison. Although this algorithm is quite far from the MCRLB (not shown here), its convergence threshold is around 15 dB.

The performance can be further improved by increasing the number of symbols N_e used for the estimation. The idea here is to use the decisions to improve the estimate accuracy in decision-directed mode. In other words, we can use the derived estimate to compensate for the Doppler rate. Detection can be thus performed. If the CRC is not correct, this is likely due to errors at the end of the packet, since the effect of an uncompensated Doppler rate will produce a large frequency deviation there. Hence, we can use some decisions at the beginning of the packet to produce, along with the nine preamble symbols mentioned earlier, a more accurate estimate. Fig. 7 provides a hint about the improvement we can obtain by increasing the value of N_e.

Since, in any case, the performance of the estimators and the minimum value of the accuracy have the same order of magnitude, especially around 15 dB, it turns out that the Doppler rate estimation is a really challenging task.

B. Receiver Numerical Results

The performance of the overall receiver in the presence of Doppler shift and Doppler rate can be now assessed. The results, in terms of PER versus the carrier-to-noise ratio (CNR) C/N, i.e., the ratio between the signal and the noise power, for different values of SF are reported in Fig. 8 and compared with that of an ideal receiver which perfectly knows the channel parameters. We considered packets of 50 symbols including the preamble and assumed that the Doppler rate and Doppler shift take on the maximum possible values for a satellite with altitude 650 km. As mentioned, when $\mathrm{SF} = 12$, Doppler rate estimation and compensation is necessary (see previous sections for insights), and the penalty due to impairments can be estimated as ∼0.3 dB at a PER $= 10^{-2}$. The transmission of a signal with $\mathrm{SF} = 10$ can be considered as borderline instead, since the maximum Doppler rate can induce a symbol shift only after ∼40 symbols. However, for values $\mathrm{SF} \leq 10$, it seems better to perform the Doppler rate estimation based on the uncompensated signal, at each iteration of the decision-directed refinement process, rather than performing it on the signal corrected in the previous iteration. This is due to errors in the estimation when there is only the small residual rate left.

TABLE III
Parameter of the Simulated Scenario

T_0	# retransm.	# runs	freq. uncert.	BW
20 s	[0 1]	2000	30 ppm	125 kHz
region	**EIRP**	**urban**	**user densities**	
EU	14 dBm	no	[0.01 0.075 0.185 0.365 0.725 1.445 2.165] users/km^2	

TABLE IV
Probability Distribution of the SF Values in the Scenario Under Study

SF	7	8	9	10	11	12
prob.	0	16/31	8/31	4/31	2/31	1/31

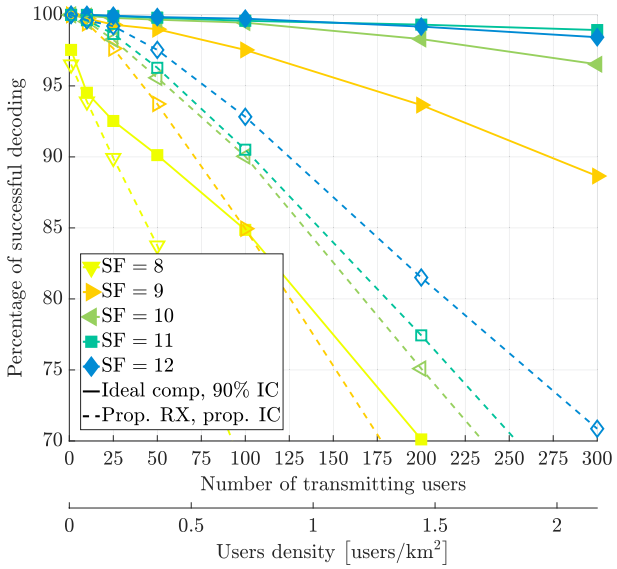

Fig. 9. Comparison between the receivers in terms of mean percentage of successfully detected packets per SF, without retransmission.

C. System Simulator Results

Finally, we report the system simulation results for the scenario depicted in Table III, where T_0 is the simulation time. Moreover, we considered that each CT transmits 12-byte packets on the 866.3 MHz channel and the SFs have a probability distribution shown in Table IV.

Though the interference arising from the packet transmissions occurs in the entire satellite FoV, the performance analysis will be restricted to a well defined geographical area (the swath) of size 1500×400 km^2 and all results (the percentage of detected packets) will be computed with reference to the number of transmitting CTs within the swath.[9]

The performance of the proposed receiver is illustrated in Figs. 9–11, where we considered the case of the absence of retransmission ($N_{\text{rep}} = 0$). These curves show how the proposed scheme is able to compensate the unknown channel impairments, almost reaching the same performance as the ideal receiver which, in case of few transmitting CTs,

[9]The number of transmitted packets is determined by the average number of messages transmitted by every terminal per day, given the IoT device class, the dimension of the swath, and the user density.

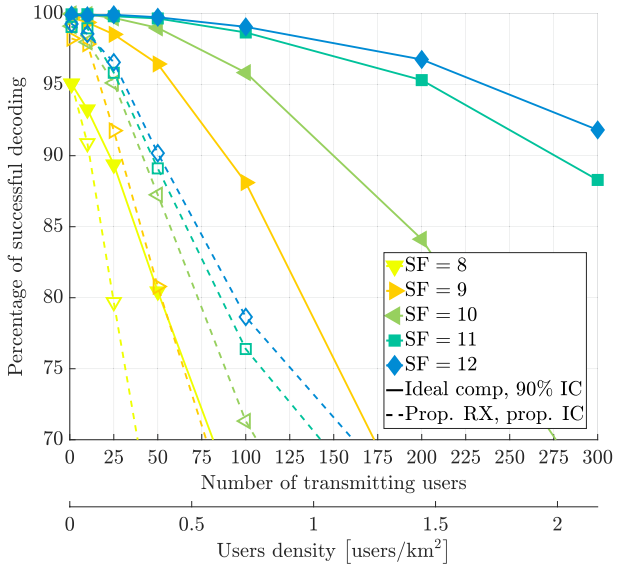

Fig. 10. Comparison between the receivers in terms of mean percentage of successfully detected packets per SF, with retransmission.

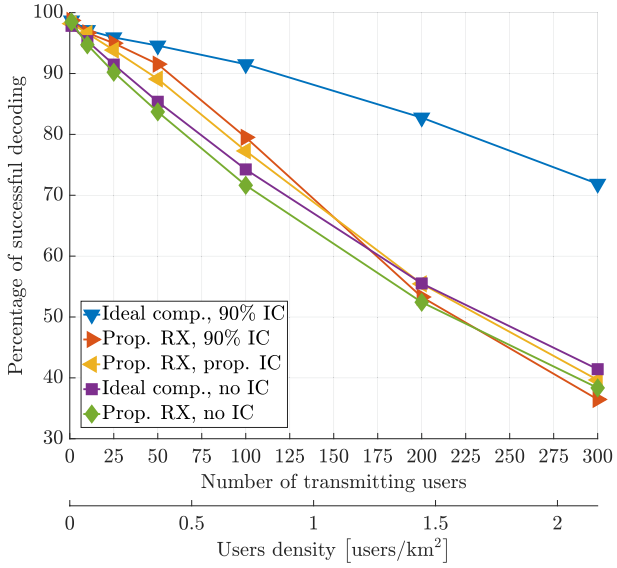

Fig. 11. Comparison in terms of mean percentage of successfully detected packets, averaged on all SFs, without retransmission.

besides perfectly compensating the channel impairments is also able to cancel at least 90% of the amplitude of each successfully detected packet. Hence, as mentioned, cancellation does not need to be perfect. When the network throughput is low, there is a limited loss between the case when 90% of the amplitude of each successfully detected packet is removed and the proposed IC. This proves that the LoRa waveform is resilient to the effects of the imperfect signal cancellation and allows to relax the precision of the estimates computed by the IC algorithm, thus reducing the complexity.

From Fig. 11, we can observe that if we give up the IC, the ideal and proposed receivers have almost the same performance. On the contrary, if we are able to cancel 90% of the amplitude of each successfully detected packet, the

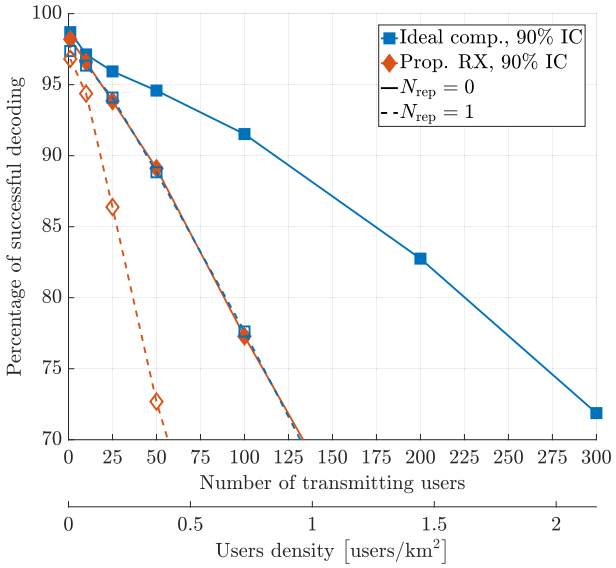

Fig. 12. Comparison in terms of mean percentage of successfully detected packets, averaged on all SFs, with and without retransmission ($N_{rep} = 1, 0$).

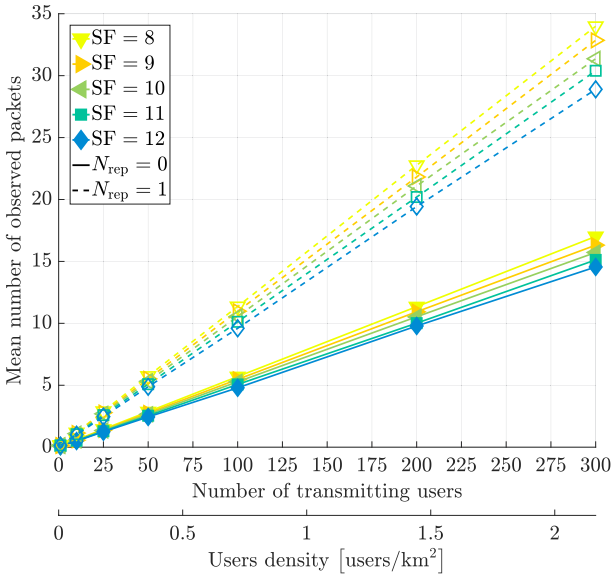

Fig. 13. Mean number of observed packets per SF, with and without retransmission ($N_{rep} = 1, 0$).

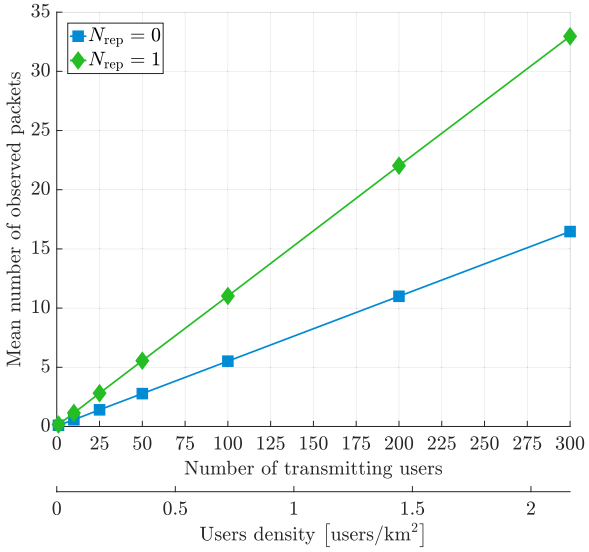

Fig. 14. Mean total number of observed packets computed overall SF values, with and without retransmission ($N_{rep} = 1, 0$).

ideal receiver with perfect estimation and compensation of the channel impairments has a much better performance than the proposed receiver. This is due to the fact that, after the (imperfect) cancellation of already detected packets, the underlying packets will have a much lower SNR, making the estimation of timing, Doppler shift, and Doppler rate much more difficult. Finally, this figure also confirms that the proposed IC performs as the ideal 90% cancellation even when averaging on all SFs.

The fast decrease of the probability of successful detection with lower SFs, shown in Fig. 10, depends on the SF probability distribution itself— the higher the probability of packets transmitted with a given SF value, the more frequent the collisions between packets with that SF value. Collisions between packets with different SF do not affect the performance thanks to their orthogonality.

If packet retransmission is introduced ($N_{rep} = 1$), the performance of both receivers worsen, as shown in Fig. 12. However, in order to evaluate the robustness of the proposed receiver, in Figs. 13 and 14 we report the amount of traffic in the LoRaWAN that the receiver must face, expressed as the mean number of observed packets in a generic time instant as a function of the number of transmitting users. Even if the number of collisions increases quickly, due to the larger number of transmitting terminals, we can observe that packets of almost 70% of the transmitting users can be decoded by the proposed receive architecture, also when more than five collisions between transmitted packets within the swath occur (actually the collisions are many more because this statistics does not take into account the collisions with packets of CTs in the FoV but outside the swath under study).

We would like to point out that all these results have been obtained by using a very simple antenna at the CT. A more sophisticated antenna would allow to obtain a larger number of decoded packets for a given user density.

VI. CONCLUSION

The problem of the coverage extension of IoT networks through the use of LEO satellites has been considered. First, we investigated the properties of the LoRa waveform and the issues concerning signal detection by a LEO satellite. Then, we proposed a new receiver architecture able to cope with the main impairments related to a LEO satellite detection, such as Doppler shift and Doppler rate and, by exploiting interference cancellation schemes, we showed that our receiver is able to significantly improve the overall network performance. Finally, we implemented a LoRaWAN network simulator and the performance of the proposed receiver in a realistic scenario has been finally assessed.

Since the proposed receiver has a very high robustness to interference, thanks also to the intrinsic robustness

of the modulation format, we can assert that it is reasonable to assume that this modulation format, when our proposed receiver is employed, is suitable for satellite-based applications.

ACKNOWLEDGMENT

The authors would like to thank Dr. A. Modenini for several inspiring discussions.

REFERENCES

[1] R. Sanchez-Iborra and M.-D. Cano
State of the art in LP-WAN solutions for industrial IoT services
Sensors, vol. 16, no. 5, 2016, Art. no. 708.

[2] S. G. Wilson
Digital Modulation and Coding. Englewood Cliffs, NJ, USA: Prentice-Hall, 1996.

[3] I. S. Gradshtein and I. M. Ryzhik
Table of Integrals, Series and Products. New York, NY, USA: Academic, 1980.

[4] S. Benedetto and E. Biglieri
Principles of Digital Transmission: With Wireless Applications. Norwell, MA, USA: Kluwer, 1999.

[5] H. Meyr, M. Oerder, and A. Polydoros
On sampling rate, analog prefiltering, and sufficient statistics for digital receivers
IEEE Trans. Commun., vol. 42, no. 12, pp. 3208–3214, Dec. 1994.

[6] G. Ferrari, G. Colavolpe, and R. Raheli
Detection Algorithms for Wireless Communications. Hoboken, NJ, USA: Wiley, 2004.

[7] A. Augustin, J. Yi, T. Clausen, and W. M. Townsley
A study of LoRa: Long range & low power networks for the internet of things
Sensors, vol. 16, no. 9, 2016, Art. no. 1466.

[8] D. C. Rife and R. R. Boorstyn
Single tone parameter estimation from discrete-time observations
IEEE Trans. Inf. Theory, vol. 20, no. 5, pp. 591–598, Sep. 1974.

[9] U. Mengali and M. Morelli
Data-aided frequency estimation for burst digital transmission
IEEE Trans. Commun., vol. 45, no. 1, pp. 23–25, Jan. 1997.

[10] LoRa Alliance, Inc., "LoRaWAN Regional Parameters," Jul. 2016. [Online]. Available: https://www.semtech.com/uploads/documents/DS_SX1276-7-8-9_W_APP_V6.pdf. Accessed on: Apr. 16, 2019.

[11] I. Ali, N. Al-Dhahir, and J. E. Hershey
Doppler characterization for LEO satellites
IEEE Trans. Commun., vol. 46, no. 3, pp. 309–313, Mar. 1998.

[12] M. Morelli
Doppler-rate estimation for burst digital transmission
IEEE Trans. Commun., vol. 50, no. 5, pp. 707–710, May 2002.

[13] G. Colavolpe, A. Barbieri, and G. Caire
Algorithms for iterative decoding in the presence of strong phase noise
IEEE J. Select. Areas Commun., vol. 23, no. 9, pp. 1748–1757, Sep. 2005.

[14] A. Barbieri and G. Colavolpe
On pilot-symbol-assisted carrier synchronization for DVB-S2 systems
IEEE Trans. Broadcast., vol. 53, no. 3, pp. 685–692, Sep. 2007.

[15] *Attenuation Due to Clouds and Fog*, Rec. ITU-R P.840-6, International Telecommunications Union, Geneva, Switzerland, 2013.

[16] *Propagation Data and Prediction Methods Required for the Design of Terrestrial Line-of-Sight Systems*, Rec. ITU-R P.530-16, International Telecommunications Union, Geneva, Switzerland, 2015.

[17] W. L. Stutzman and G. A. Thiele
Antenna Theory and Design, 3rd ed. Hoboken, NJ, USA: Wiley, 2012.

[18] Semtech Corporation, "SX1276/77/78/79–137 MHz to 1020 MHz Low Power Long Range Transceiver," 2015. [Online]. Available: https://www.semtech.com/uploads/documents/DS_SX1276-7-8-9_W_APP_V6.pdf. Accessed on: Apr. 16, 2019.

[19] A. N. D'Andrea, U. Mengali, and R. Reggiannini
The modified Cramer–Rao bound and its application to synchronization problems
IEEE Trans. Commun., vol. 42, no. 2, pp. 1391–1399, Feb. 1994.

Giulio Colavolpe (S'96–M'00–SM'11) was born in Cosenza, Italy, in 1969. He received the Dr. Ing. degree in telecommunications engineering (cum laude) from the University of Pisa, Pisa, Italy, and the Ph.D. degree in information technologies from the University of Parma, Parma, Italy, in 1994 and 1998, respectively.

Since 1997, he has been with the University of Parma, where he is now Professor of Telecommunications with the Dipartimento di Ingegneria e Architettura (DIA). In 2000, he was Visiting Scientist with the Institut EurÃl'com, Valbonne, France. His research activity has led to more than 200 papers in refereed journals and in leading international conferences, and 18 industrial patents. His research interests include the design of digital communication systems, adaptive signal processing (with particular emphasis on iterative detection techniques for channels with memory), channel coding and information theory.

Prof. Colavolpe is the recipient of the Best Paper Award at the 13th International Conference on Software, Telecommunications and Computer Networks (SoftCOM'05), Split, Croatia, September 2005, the Best Paper Award for Optical Networks and Systems at the IEEE International Conference on Communications (ICC 2008), Beijing, China, May 2008, and the Best Paper Award at the Fifth Advanced Satellite Mobile Systems Conference and 11th International Workshop on Signal Processing for Space Communications (ASMS&SPSC 2010), Cagliari, Italy. He was an Editor for IEEE TRANSACTIONS ON WIRELESS COMMUNICATIONS, IEEE TRANSACTIONS ON COMMUNICATIONS, and IEEE WIRELESS COMMUNICATIONS LETTERS and an Executive Editor for *Transactions on Emerging Telecommunications Technologies* (ETT).

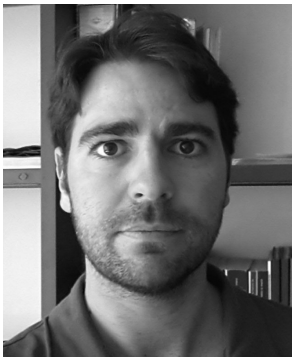

Tommaso Foggi received the Dr. Eng. degree in telecommunication engineering and the Ph.D. degree in information technology from the University of Parma, Parma, Italy, in 2003 and 2008, respectively.

In 2004, he was with the Photonic Networks and Technologies Nat'l Lab in Pisa. From 2009 to 2018, he was a Research Engineer with the National Inter-University Consortium for Telecommunications (CNIT) of the University of Parma Research Unit. He is now a Research Associate with the Engineering and Architecture Department of the University of Parma. He is author of more than 50 peer-reviewed papers and several patents. His main research interests include electronic signal processing for optical communication systems, in particular adaptive equalization, coding and iterative decoding techniques, optical channel impairment compensation, channel estimation, simulative software implementation.

Dr. Foggi is the recipient of the Best Paper Award at the Optical Networks and Systems Symposium at the IEEE International Conference on Communications (ICC 2008), Beijing, China, May 2008.

Michelangelo Ricciulli was born in Foggia, Italy, in 1989. He received the Dr. Eng. degree cum laude in telecommunications engineering and the Ph.D. degree in information technologies from the University of Parma, Parma, Italy, in 2014 and 2018, respectively.

In 2017, he was a Visiting Student with Lund University, Sweden, where he developed a project funded by the European Space Agency. He is currently an Engineer with an R&D Department for Wireless Transmission Systems, Nokia, Vimercate, Italy. His main research interests include digital communications, information theory, and digital signal processing applied to both wireless and optical systems.

Yuri Zanettini was born in Parma, Italy, in 1986. He received the Dr. Eng. degree in telecommunications engineering in October 2014 and the Ph.D. degree in information technologies, both from the University of Parma, Parma, Italy.

He has been a Member of the Signal Processing for Advanced Digital Communications Lab (SPADiC Lab), and had worked on the Project "OPtimized transmission TechnIques for satcoM UnicaSt interactive traffic" (OPTIMUS), funded by the European Space Agency (ESA-ESTEC), and on the Project "Inmarsat Communication Evolution," funded by Inmarsat. He is currently an Engineer with the High-Speed Optics Division, Nokia, Vimercate, Italy. His main research interests include optical and satellite communications, advanced digital signal processing and synchronization.

Juan-Pedro Mediano-Alameda was born in Jaén, Spain, in 1983. He received the M.Sc. in telecommunications engineering (cum laude) from the University of Málaga, Málaga, Spain, in 2007, and the M.Res. in telecommunications engineering in 2010.

In 2007, he started his career as a System Analyst with the Communications and High Technology Division, Accenture. In 2010, he joined the French Space Agency (CNES) in Toulouse, France, as Satellite Communications Engineer. In 2011, he joined SSTL, U.K., as Technical Lead of several subsystems of the Galileo satellites and later, in 2014, he worked as Senior Satellite Systems Engineer for the Satellite Applications Catapult in Harwell, U.K. Since 2015, he has been working as a Senior Satellite Systems Architect for Inmarsat in London.